J Chin Med Assoc

ORIGINAL ARTICLE

Effects of polyallylamine-coated nanoparticles on the optical and photochemical properties of rose bengal

Kai-Ying Lin[a], Yeou-Guang Tsay[a,b,c,*], C. Allen Chang[c,d,e,f]

[a]Department of Biotechnology and Laboratory Science in Medicine, National Yang Ming Chiao Tung University, Taipei, Taiwan, ROC; [b]Institute of Biochemistry & Molecular Biology, National Yang Ming Chiao Tung University, Taipei, Taiwan, ROC; [c]Metabolomics–Proteomics Research Center, National Yang Ming Chiao Tung University, Taipei, Taiwan, ROC; [d]Biomedical Engineering Research and Development Center (BERDC), National Yang Ming Chiao Tung University, Taipei, Taiwan, ROC; [e]Department of Biomedical Imaging and Radiological Sciences, National Yang Ming Chiao Tung University, Taipei, Taiwan, ROC; [f]Biophotonics & Molecular Imaging Research Center (BMIRC), National Yang Ming Chiao Tung University, Taipei, Taiwan, ROC

Abstract

Background: Inasmuch as optical and photochemical properties of a photosensitizer can be modified upon association with the nanoparticle (NP), we wondered whether the effectiveness of phototherapeutic rose bengal (RB) was affected upon tethering to the sodium lanthanide fluoride NP with an outer polyallylamine (PAH) coat.

Methods: RB molecules were electrostatically bound to the $NaYF_4$:Gd^{3+}:Nd^{3+}NPs with inner silica and outer PAH coats. The products were analyzed for their size, shape and zeta potential using transmission electron microscopy and dynamic light scattering instrument. Ultraviolet–visible absorption spectrometry and fluorescence spectrometry were used to examine the spectral properties. Photodynamic effect in terms of singlet oxygen generation was quantitatively determined using the indicator 1,3-diphenylisobenzofuran (DPBF). Photocytotoxicity mediated by NP-bound RB was tested using A549 cells (Student's *t* test was used for statistical evaluation).

Results: NP-bound RB had the major absorbance peak at 561 nm, in comparison with 549 nm for free RB, accompanied with a significant decrease in absorptivity. The molar extinction coefficient becomes 36 000 M^{-1} cm^{-1}, only ~35% of that for free RB. Fluorescence spectral analyses showed a paradoxical decrease in the emission with higher NP concentrations even at very low dilutions. Most importantly, the association of RB with these NPs drastically increased its singlet oxygen production upon irradiation. The interaction of RB with PAH coat could partly account for this enhancement, given our finding that PAH in solution also caused a drastic rise in DPBF reactivity by free RB. These NPs exhibited strong photocytotoxic effects, and their promise in photodynamic therapy was addressed.

Conclusion: Our findings provide evidence that the PAH coat plays a key role in enhanced biological activities of RB delivered via NPs, including the increase in singlet oxygen production and photocytotoxic effects.

Keywords: Lanthanoid series elements; Nanoparticles; Photochemotherapy; Polyallylamine; Rose bengal; Singlet oxygen

1. INTRODUCTION

Photodynamic therapy (PDT) has emerged as an important therapeutic option for cancer.[1] Rose bengal (RB) is a well-known photosensitizer, having a quantum yield of 76% irradiated with 532 nm light.[2] However, RB suffers from poor intracellular uptake and tends to aggregate in solution at concentrations above 50 μM, which limits its use in biomedical applications.[3] Recently, the advantages of nanoparticles (NPs) as a vehicle for conjugation with RB to reduce aggregation,[4] to enhance the uptake efficiency by cancer cells,[5] and to achieve photothermal therapy and PDT[2] have been reported.

Interestingly, it has been reported that both binding to silicon dioxide (SiO_2) NPs itself and increasing the number of adsorbed dye molecules can cause significant fluorescence quenching with a shortening of the fluorescence lifetime of the Atto 532.[6] NPs can affect dye fluorescence in solution through multiple pathways, including the fluorescence inner filter effect, dynamic quenching, static quenching, surface enhancement, and fluorophore quantum yield variation. These effects are associated with the structural and conformational changes induced by NP binding.[7] On the other hand, the nature of the interactions between the dye and solvent and between the dye and solid determines the partition equilibrium of the dye and the degree of aggregation. In addition, there may be slight variations in the saturation number of dye molecules adsorbed because of steric hindrance.[8]

NPs composed of the Nd^{3+} and Gd^{3+} have been chosen based on the potential use as the contrast agents for both magnetic resonance imaging (MRI)[9] and near infrared (NIR) fluorescence.[10] A

*Address correspondence. Dr. Yeou-Guang Tsay, National Yang Ming Chiao Tung University, 155, Section 2, Linong Street, Taipei 112, Taiwan, ROC. E-mail address: tsayyeou@nycu.edu.tw (Y.-G. Tsay).

Conflicts of interest: The authors declare that they have no conflicts of interest related to the subject matter or materials discussed in this article.

Journal of Chinese Medical Association. (2022) 85: 901-908.

Received March 4, 2022; accepted May 5, 2022.

doi: 10.1097/JCMA.0000000000000762.

cationic polyelectrolyte polyallylamine (PAH) is used to modify the silica-shelled surface of the NPs to obtain a high loading of RB and improve the biocompatibility.[11] Here, we characterized the optical properties and documented the optimal conditions for $^1O_2$ generation efficiency of RB on PAH-coated NPs.

2. METHODS

2.1. Chemicals and reagents

The following were from Sigma-Aldrich (USA): yttrium(III) acetate hydrate ($(CH_3CO_2)_3Y{\cdot}xH_2O$), gadolinium(III) acetate hydrate ($Gd(CH_3CO_2)_3{\cdot}xH_2O$), neodymium(III) acetate hydrate ($(CH_3CO_2)_3Nd{\cdot}xH_2O$), oleic acid (OA, 90%), octadecene (ODE, 90%), sodium hydroxide (NaOH, 99.99%), ammonium hydroxide solution (NH_4OH, 28.0%–30.0%), ammonium fluoride (NH_4F, ≥ 99.99%), IGEPAL CO-520, and poly(allylamine) hydrochloride solution (PAH, average M_W ≈17 000, 20 wt.% in H_2O), RB (dye content 95%, M_W = 1017.64), 1,3-diphenylisobenzofuran (DPBF), phosphate-buffered saline (PBS, Sigma), Dulbecco's Modified Eagle's medium (DMEM, high glucose), trypan blue solution, and 3-(4,5-dimethylthiazol-2-yl)-2,5-diphenyltetrazolium bromide (MTT)-formazan. ACS-grade methanol (MeOH), acetone, ethanol (EtOH, 99.9%), and hexane were from Fischer (USA). Tetraethyl orthosilicate (TEOS, 98%) was from Acros (USA). Trypsin-ethylenediaminetetraacetic acid (EDTA, 0.25%) and fetal bovine serum (FBS) were from Gibco (USA). Penicillin, streptomycin, amphotericin B (P/S/A) mixture and Cell Counting Kit-8 (CCK-8) were from Biological Industries (Cromwell, Connecticut, USA) and Enzo Life Sciences, Inc. (Farmingdale, NY, USA), respectively. All organic solvents and chemical reagents were used without further purification.

2.2. Instrumentation

The size and shape of the NPs were characterized by a transmission electron microscope (TEM) JEM-2000EXII (JEOL, Akishima, Japan) with an acceleration voltage of 100 kV. The statuses in solution were determined using a HORIBA SZ-100 (Kyoto, Japan) dynamic light scattering (DLS) instrument at room temperature. The ultraviolet–visible (UV-Vis) absorbance intensity was measured using Hewlett-Packard model 8453 (Agilent Technologies, Santa Clara, USA). Steady-state fluorescence (FL) spectra were obtained using an FSP920 spectrometer (Edinburgh Instruments, Livingston, United Kingdom). A multimode microplate reader Infinite 200 (Tecan, Männedorf, Switzerland) was used for absorption and fluorescence measurements, which gave absorption MRab and fluorescence MRfl measurements, respectively. An Olympus CKX41 microscope was used in in vitro tests.

2.3. Synthesis of $NaYF_4$:Gd,Nd NPs

NPs were prepared following a reported method with some modification.[12] A solution containing 8 mL of OA and 12 mL of ODE, $Y(COOCH_3)_3{\cdot}4H_2O$ (0.7 mmol), $Gd(COOCH_3)_3{\cdot}4H_2O$ (0.27 mmol), and $Nd(COOCH_3)_3{\cdot}4H_2O$ (0.03 mmol) was stirred vigorously for 30 minutes at 190°C in a two-necked round-bottom flask with argon flow. As cooled to 70°C, 5 mL of methanol containing NH_4F (4 mmol) and NaOH (2.5 mmol) was added. The temperature was then increased to 300°C and maintained for 100 minutes with vigrous stir. The precipitate was formed in acetone centrifuged at 4000 rpm for 5 minutes. Finally, the precipitate was washed with ethanol and dispersed in hexane.

2.4. Surface modification process

2.4.1. $NaYF_4$:Gd,Nd@SiO_2

The procedure was primarily based on previous reports.[13] First, 1.4 mL IGEPAL CO-520 was mixed with 36 mg NPs (in 28 mL hexane) and 0.2 mL ammonia solution. After sonication, TEOS (0.3 mL) was added by a syringe pump, and the solution was stirred for 18 hours. MeOH was then added for precipitation. After washing three times and centrifuging at 12 000 rpm for 20 minutes each with EtOH, the silica-coated NPs were dispersed in EtOH.

2.4.2. $NaYF_4$:Gd,Nd@SiO_2@PAH (PAH-NP)

A PAH coating procedure was reported previously with modification.[14] Initially, 350 μL of PAH was added to 15 mg of silica-coated NPs in 15 mL EtOH and stirred for 6 hours. The particles were harvested by centrifugation at 12 000 rpm for 20 minutes and then washed three times as described above. Finally, the positively charged particles were dispersed in distilled water.

2.4.3. $NaYF_4$:Gd,Nd@SiO_2@PAH@RB (RB-NP)

Serial amounts of negatively charged RB (X = 0.01, 0.02, 0.05, 0.1, 0.15, 0.2, 0.3, 0.4, 0.5, 0.6, 0.8 and 1 mg) were added to 2 mg PAH-NP solution, denoted NX. The reaction continued for 12 hours at room temperature with stir. After a series of washing and centrifugation, the RB-NPs were dispersed in distilled water and stored at 4°C.

2.5. Quantification of NP-bound RB molecules

The calibration curves (λ_{ab} = 549 nm) were constructed using 1.5-fold serial dilutions of the RB solutions. The number of RB molecules on the NP was calculated by subtracting the unbound RB from the total added one. For comparison, the absorbance of RB-NPs (λ_{ab} = 561 nm) was also recorded by UV-Vis to obtain the extinction coefficient of NP-bound RB.

2.6. Determination of the absorption and fluorescence behavior

The fluorescence and absorption spectra of the RB solution were recorded with or without 0.018 μM of PAH, and RB-NP solutions (0.1 mg NPs/mL).

2.7. Evaluation of $^1O_2$ generation

Singlet oxygen generation was analyzed by monitoring the decrease in the absorbance of DPBF at 417 nm with slight modifications.[15] A stock solution of DPBF in dimethyl sulfoxide (DMSO) and 10 μL of DPBF were added to 2 mL of distilled water. A solution containing 70 μM DPBF and with free RB, 3 μL of PAH or RB-NPs (0.05 mg NPs/mL) was analyzed using a fluorescence spectrometer equipped with the xenon lamp.

2.8. In vitro tests

2.8.1. Cell culture

Human lung carcinoma cell line A549 with passage number of 103 (CCL-185, American Type Culture Collection) was a gift from the Laboratory of Hsin-Ell Wang, Department of Biomedical Imaging and Radiological Sciences, National Yang Ming Chiao Tung University, Taiwan. The cells were maintained in DMEM supplemented with 10% FBS and 100 U/mL P/S/A in a humidified atmosphere containing 5% CO_2 at 37°C.

2.8.2. Cytotoxicity

A549 cells were seeded in 96-well plates at a density of 1×10^5 cells/mL. The PAH-NPs were incubated with cells overnight and then washed. After incubation for 4 hours with MTT (0.5 mg/mL), the formazan crystals were dissolved in 100 μL of isopropanol and then recorded at 570 nm.

2.8.3. Photocytotoxicity

A549 cells were seeded and treated with either RB or RB-NPs for 4 hours after overnight incubation. Before exposure to ambient light (a 30 W white light source in a laminar flow cabinet, Tsao Hsin VCM-420) for 30 minutes at a fixed distance of 70 cm, the cells were washed three times with PBS. After incubation for 2 hours with CCK-8, the absorbance was detected at 450 nm with reference to that at 650 nm. A trypan blue exclusion assay was performed for confirmation.

3. RESULTS

3.1. Properties and characterization of the synthesized NPs

The $NaYF_4$:27%Gd^{3+},3%Nd^{3+} NPs were monodispersed spheres (Fig. 1A). When coated with silica (Fig. 1B), these particles had the size of 22 nm using TEM, and 86.8 ± 16.9 nm with zeta potential of –63.0 ± 3.3 mV using DLS. After modification with PAH, the zeta potential became positive (+60.8 ± 1.8 mV) and the fluorescence intensity weakened (Fig. 2).

3.2. Absorption and fluorescence behavior

NP-bound RB molecules were estimated and compared (Fig. 3A). The calibration curve of RB-NPs was determined based on a linear relationship between absorbance and concentration (Fig. 3B). The solutions of free RB had a molar extinction coefficient of 100 000 M^{-1} cm^{-1} at 549 nm, whereas those of NP-bound RB exhibited a lowered coefficient of 36 000 M^{-1} cm^{-1} at 561 nm. The results by different instruments were listed in Table 1.

With peaks at 549 and 512 nm for water-soluble RB (Fig. 4A), there were redshifts to 561 and 525 nm for the NP-bound RB (Fig. 4B) as well as a decrease in the signal intensity. This redshift was also found in RB in the presence of PAH (RB-PAH, Fig. 4C), while the peak-to-shoulder ratio is closer to that of free RB, with no decrease in intensity. The peak-to-shoulder ratios of our RB-NP preparations, which ranged from 1.26 to 1.72, were closest to those of free RB at high concentrations as 44–67 μM (Tables 2 and 3).

Redshifts were observed in the fluorescence spectra of the free RB and NP-bound RB from 565 to 575 nm and from 579 to 591 nm respectively (Fig. 5A, B). The fluorescence intensity showed a constant decrease in NP-bound RB as more RB bound to NPs, in contrast to a bimodal behavior of free RB.

3.3. Evaluation of the $^1O_2$ generation of RB-NPs

Upon irradiation, DPBF was consumed in the presence of either 13 μM of RB or the RB-saturated RB-NPs, and half of the DPBF disappeared within 30 minutes in the latter (Fig. 6A). At a fixed NP dose, the DPBF consumption increased dependent on the concentration of NP-bound RB. For RB and NP-bound RB at 13 μM, the former consumed less than 20% of the DPBF, whereas approximately 50% was converted in the presence of the latter (Fig. 6B). For the same amount of NP-bound RB in the reaction, the presence of more NPs results in a lower RB density over the NP surface. At RB density higher than a certain threshold, an apparent DPBF consumption was observed (Fig. 6C). In the presence of PAH in solution, 0.2 and 13 μM of RB consumed 40% and 70% of DPBF, respectively (Fig. 6D).

3.4. In vitro photocytotoxicity tests with RB-NPs

Upon treatment of A549 with PAH-NPs, a dose-dependent cytotoxicity effect could be observed (Fig. 7A). Compared to free RB in solutions, RB-NPs with the concentration of 33, 65, and 130 μM of NP-bound RB inhibited cell viability by 15.8%, 16.7%, and 21.6%, respectively (Fig. 7B). Trypan blue exclusion assays was used for visualization (Fig. 7C).

4. DISCUSSION

The characteristic emissions of Nd^{3+} were observed at 900, 1057, and 1330 nm.[16] The absorptivity of lanthanides is very low (< 10 M^{-1} cm^{-1}).[17] This should limit the energy transfer from surface RB to the NP core, although there is an overlap between the emission of RB and excitation of the NPs at 574 nm. The RB molecules were electrostatically bound to the oppositely charged surface of the NPs. This type of modification can reduce leaching when compared to silica encapsulation, covalent conjugation, physical adsorption, and direct surface coating.[18]

Our data suggest that PAH binding contributes to the observed redshift of NP-bound RB. Some proposed the interaction with amine-containing polymers may induce the planarization of the RB molecule, underlying the changes in spectral properties.[4] The peak-to-shoulder ratio is related to the level of aggregation.[19] Given no change of this ratio for RB-PAH as RB (Fig. 4C), the lower value seen for NP-bound RB is likely a result of so-called nanosized confinement.[6] It has been reported that RB molecules can dimerize on oppositely charged surfaces of NPs.[20] Some researchers hypothesize that positively charged particles are more compact and contain less water, which helps RB concentrate at the particle surface.[21] In another example, a severe decrease in absorption and a higher degree of dimerization were reported for PAH-RB-PAH-coated NPs.[22] Since our data showed that NP-bound RB could reduce the fluorescence intensity more effectively than free RB, NP appears to further augment the inner filter effect of RB. This may limit the use of fluorescence of NP-bound RB.

To date, there have been few studies of the changes in photochemical properties of photosensitizers upon association with NPs.[23] In one example, RB conjugated to the PAH coat by

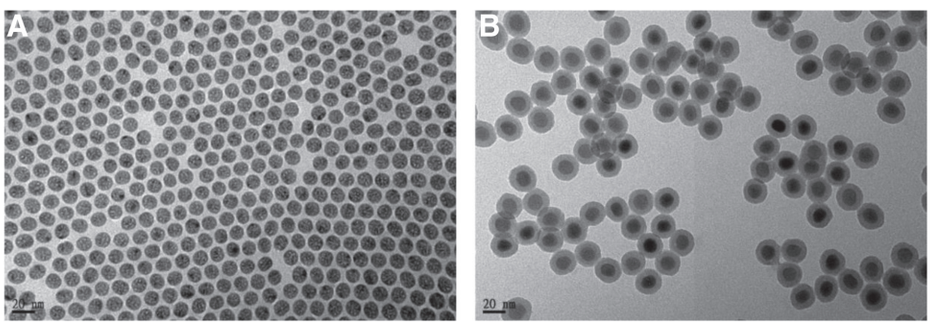

Fig. 1 Imaging analysis of the synthesized sodium lanthanide fluoride NPs. TEM (operating voltage: 100 kV) images of core $NaYF_4$:27%Gd^{3+},3%Nd^{3+} NPs (A) and silica-shelled NPs (B). Scale bars are 20 nm. NP = nanoparticle; TEM = transmission electron microscope.

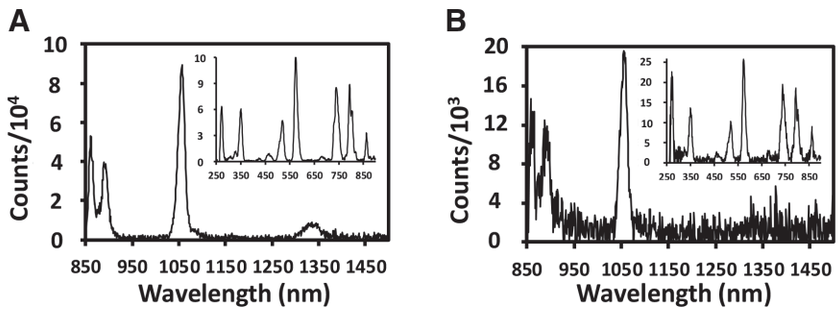

Fig. 2 Fluorescence spectra of the synthesized sodium lanthanide fluoride NPs. Emission spectra (λ_{ex} = 793 nm) of bare core NPs (A) and PAH-modified NPs (B). Insets are excitation spectra (λ_{em} = 1057 nm). NP = nanoparticle; PAH = polyallylamine.

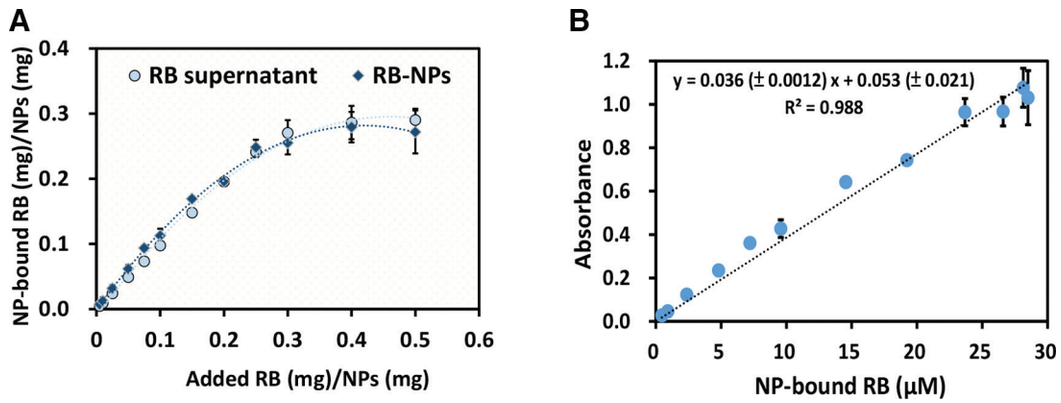

Fig. 3 RB present on RB-NPs prepared by mixing different amounts of RB and a fixed mass of NPs. A, The amount of NP-bound RB was quantitatively determined by subtraction of the RB concentration in the supernatant from that of total RB (circles). The concentration of NP-bound RB was also determined using the calibration curve of RB-NPs (diamonds) for comparison. No significance was observed between these two methods: indirect calculation by supernatant or direct evaluation by RB-NPs (p = 0.012). The saturation point was estimated at 0.25 mg RB/mg NP (N0.5) by both data sets. Calibration curve of RB-NPs (B) was established based on the absorption (λ_{ab} = 561 nm) of RB-NPs using a 0.1 mg/mL RB-NP stock solution. The concentration of NP-bound RB was obtained through subtraction of the concentration of free RB from that of total RB added to the solution. n = 6 experiments, mean ± SD. NP = nanoparticle; RB = rose bengal.

Table 1

Limit of detection and linear range of RB and RB-NPs in solution obtained by UV-Vis, FL, MR_{ab}, or MR_{fl} measurements

Parameters	UV-Vis	FL	MR_{ab}	MR_{fl}
Condition of detection (nm)				
RB-NPs	λ_{ab} = 561	λ_{ex} = 561, λ_{em} = 579	λ_{ab} = 561	N/A
RB	λ_{ab} = 549	λ_{ex} = 549, λ_{em} = 567	λ_{ab} = 549	λ_{ex} = 540, λ_{em} = 570
Limit of detection (μM)				
RB-NPs	0.0176	0.0873	0.0476	N/A
RB	0.00745	0.000387	0.0168	0.0167
Linear range (μM)				
RB-NPs	0.465–28.5	0.465–14.6	0.465–28.5	N/A
RB	0.152–13.2	0.0451–0.514	0.457–59.3	0.203–2.31

Limit of detection: signal-to-noise ratio = 3; linear range was defined as CV < 15% (n = 3). The total volumes of the solutions used for detection were 2.1 mL for UV-Vis, 1 mL for FL, and 0.1 mL for MR measurements.

CV = coefficient of variation; FL = fluorescence; N/A = not applicable; NP = nanoparticle; RB = rose bengal; UV-Vis, ultraviolet–visible.

covalent linkage, the peak of redshift is at 558 nm with a peak-to-shoulder ratio of 1.5, and the triplet lifetime is shortened and $^1O_2$ production decreases.[24] Our data indicate that free RB in PAH solution is sufficient to enhance $^1O_2$ production but with a slight decrease in high dose of RB upon excitation, and NP-bound RB (N0.5) has a lower capacity for $^1O_2$ production (Fig. 6D). The decrease in $^1O_2$ production by NP-bound RB may be due to two reasons. First, the nanosized confinement conferred by the NP surface reduces the production by NP-bound RB. Second, the aggregation/dimerization of RB is much more prevalent in the NP-bound RB versus RB in PAH solution (Fig. 4C). This is consistent with the report that aggregation/dimerization may not necessarily lead to better PDT efficacy.[25] In addition, for a fixed amount of NP-bound RB (Fig. 6C), the increased consumption

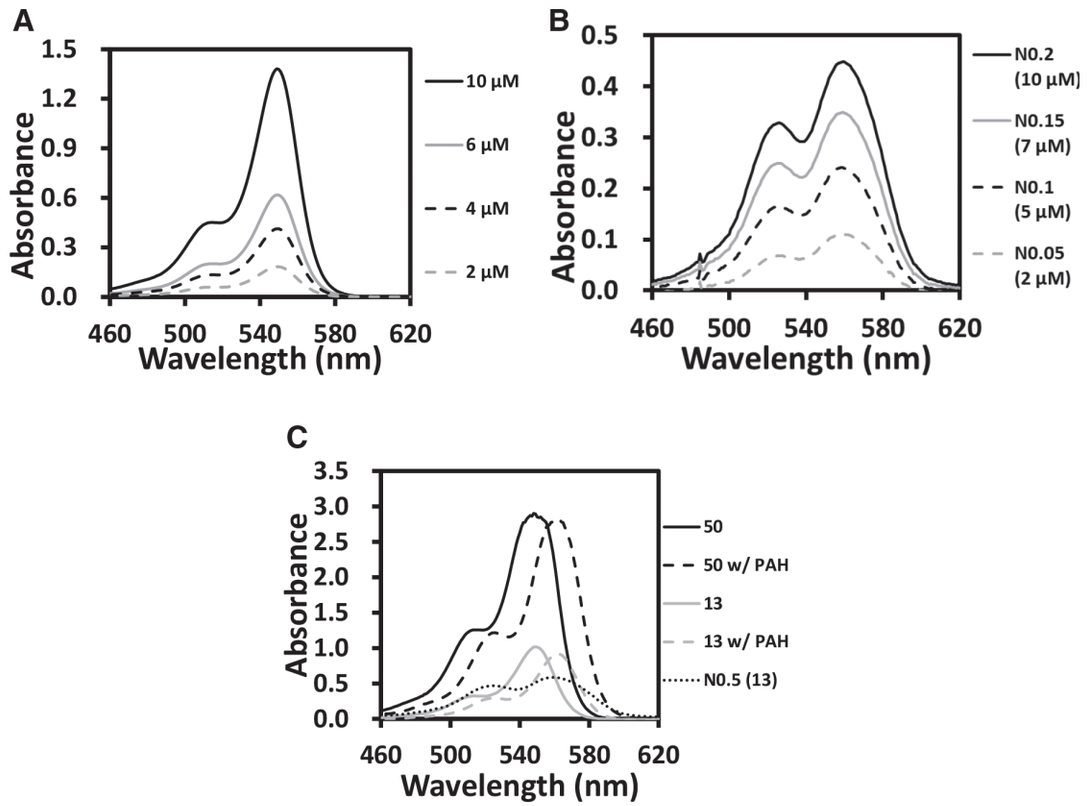

Fig. 4 Absorption spectra of RB, RB-PAH, and RB-NPs. Absorption spectra of RB (A) and RB-NPs (B). The concentrations of RB-NPs used were both 0.1 mg NPs/mL. The estimated RB concentrations in the parentheses of the RB-NPs are based on Figure 3A. C, RB at 13 or 50 μM with and without 0.018 μM of PAH were analyzed, and N0.5 (RB-NPs) was used in parallel experiments. The concentration of RB-NPs used was 0.05 mg/mL. Parentheses indicate the concentration of NP-bound RB (μM). The λ_1/λ_2 absorption ratios (549 nm/512 nm) of 13 and 50 μM free RB solutions are 3.16 and 2.32, respectively, and the λ_1/λ_2 ratios (561 nm/525 nm) of 13 and 50 μM of RB-PAH are 3.15 and 2.32, respectively. The ratio of λ_1/λ_2 (561 nm/525 nm) of N0.5 RB-NPs is 1.25 (λ_1: maximum, λ_2: shoulder). NP = nanoparticle; PAH = polyallylamine; RB = rose bengal.

Table 2

Peak-to-shoulder (λ_1/λ_2) absorption ratio (549 nm/512 nm) of free RB (λ_1: maximum, λ_2: shoulder)

Free RB	Linear range															
Concentration (μM)	100	67	44	30	20	13	8.8	5.9	3.9	2.6	1.7	1.2	0.77	0.51	0.34	0.23
Intensity ratio (λ_1/λ_2)	1.05	1.43	2.07	2.78	3.04	3.09	3.10	3.10	3.10	3.11	3.11	3.11	3.10	3.12	3.11	3.13

RB = rose bengal.

Table 3

Peak-to-shoulder (λ_1/λ_2) absorption ratio (561 nm/525 nm) of RB-NPs (λ_1: maximum, λ_2: shoulder)

RB-NPs	N1	N0.8	N0.6	N0.5	N0.3	N0.15	N0.05	N0.01
NP-bound RB (μM)	27	27	25	24	15	7.3	2.4	0.47
Intensity ratio (λ_1/λ_2)	1.26	1.25	1.25	1.26	1.30	1.37	1.50	1.72

NP = nanoparticle; RB = rose bengal.

of DPBF results from the compact packing of RBs on the PAH-coated NP surface but not from RB binding to NP surface. Also, the core material is probably independent of this effect, since RB bound to barium titanate NPs coated with PAH also showed similar photocytotoxic effect.[22] These results support our conclusion that RB interaction with PAH coat via electrostatic interaction leads to this $^1O_2$ enhancing effect.

While PAH is generally considered to be an inert vehicle for the delivery of bioactive substances,[26,27] our studies, in line with the others, observed that the PAH coat over NPs indeed shows unexpected cytotoxicity like other similar studies. It has been speculated that high concentration of positive charge over the NP coat may account for such effects.[28,29] Nevertheless, it is important to recognize that, when the sodium lanthanide fluoride NPs with the positively charged coat was given to model animals, there was no noticeable in vivo toxicity for normal organs, with apparent suppression of tumor tissues.[30] The difference in the permeability of the vessels, or enhanced permeability

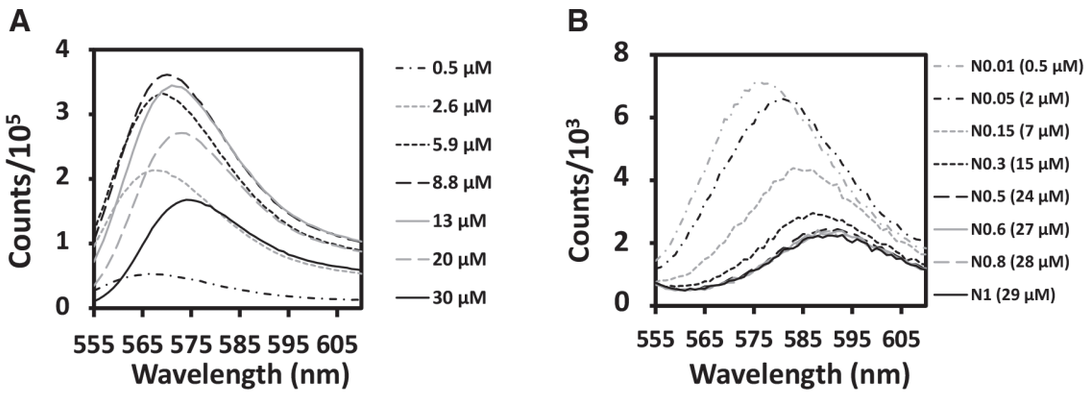

Fig. 5 Fluorescence spectra of RB and RB-NPs. Fluorescence spectra of serial dilutions of RB (A) and RB-NPs (B) in solution. NP = nanoparticle; RB = rose bengal.

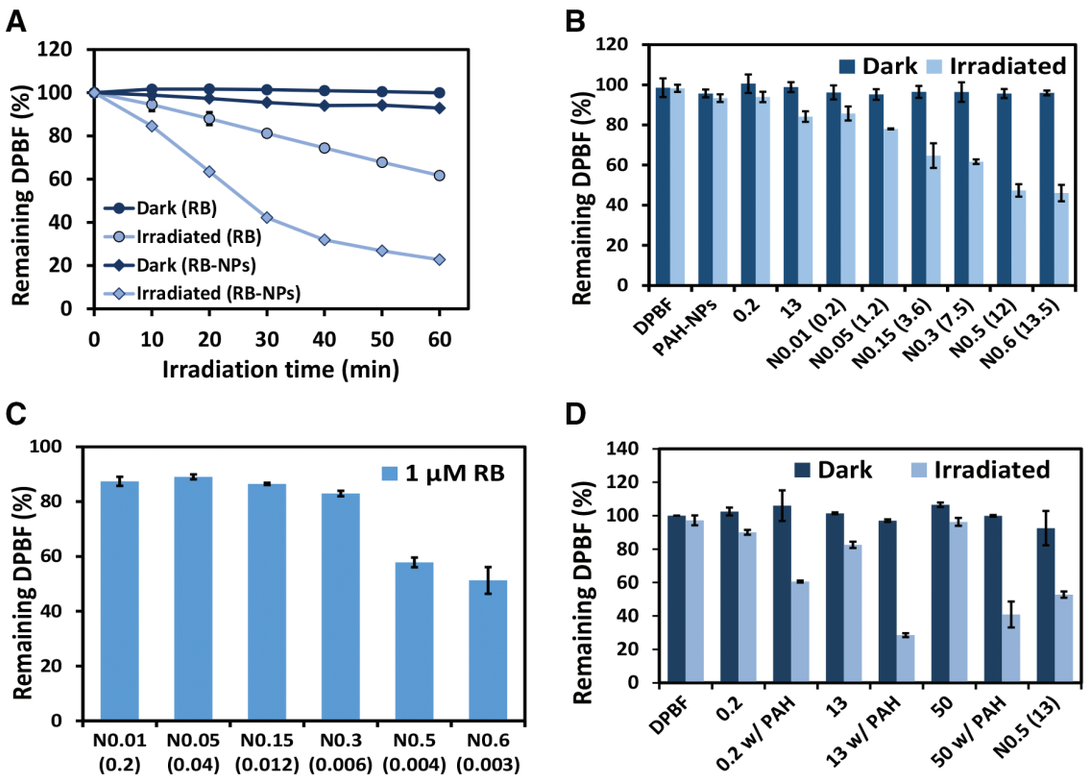

Fig. 6 Evaluation of singlet oxygen generation. A, RB (13.1 μM) and RB-saturated RB-NPs (N0.8) with and without irradiation by an 8-mW/cm^2 xenon lamp (λ_{ex} = 549 nm for RB, and λ_{ex} = 561 nm for RB-NPs) for the indicated time (n = 2). B, $^1O_2$ generation was detected for RB (λ_{ex} = 549 nm) and RB-NPs (λ_{ex} = 561 nm) with an irradiation time of 30 min. DPBF only and PAH-NPs served as controls (n = 3). C, A group of solutions with different amounts of RB-NPs equivalent to 1 μM RB were irradiated at 561 nm for 15 min. Parentheses indicate the concentration of RB-NPs (mg/mL) used for analysis (n = 2). D, An RB solution (0.2, 13, or 50 μM) with and without 3 μL of PAH was analyzed for singlet oxygen production (n = 2). N0.5 (RB-NPs) was used for comparison. The concentration of RB-NPs used was 0.05 mg/mL. Parentheses indicate the concentration of NP-bound RB (μM). Data are mean ± SD. DPBF = 1,3-diphenylisobenzofuran; NP = nanoparticle; PAH = polyallylamine; RB = rose bengal.

and retention effect, has been attributed to the specific effects on tumor tissues,[31] which is also the reason why NPs are considered to be the preferred vehicles for the delivery of reagents like RB.

Even with the expected inertness for normal tissues in vivo, there have been some efforts to change the outer coat properties for the decrease in PAH bioactivity. For example, polyethylene glycol has been added to the outer coat for the decrease in the density of positively charged PAH.[32] Researchers have also attempted to modified the coats with ligands for specific recognition of tumor cells[33] or chemicals for pH-sensitive release based on the unique microenvironment of cancer tissues.[29] To further our results for the development of clinical theragnostic materials, we will examine these possibilities to enhance the tumor-specific uptake of RB-bound NP with PAH coats.

In conclusion, RB on the surface of $NaYF_4$:Gd,Nd@SiO_2@PAH influences its optical and photochemical properties. Most importantly, the interaction of RB with the PAH coat can partly account for the enhancement of $^1O_2$ production. The

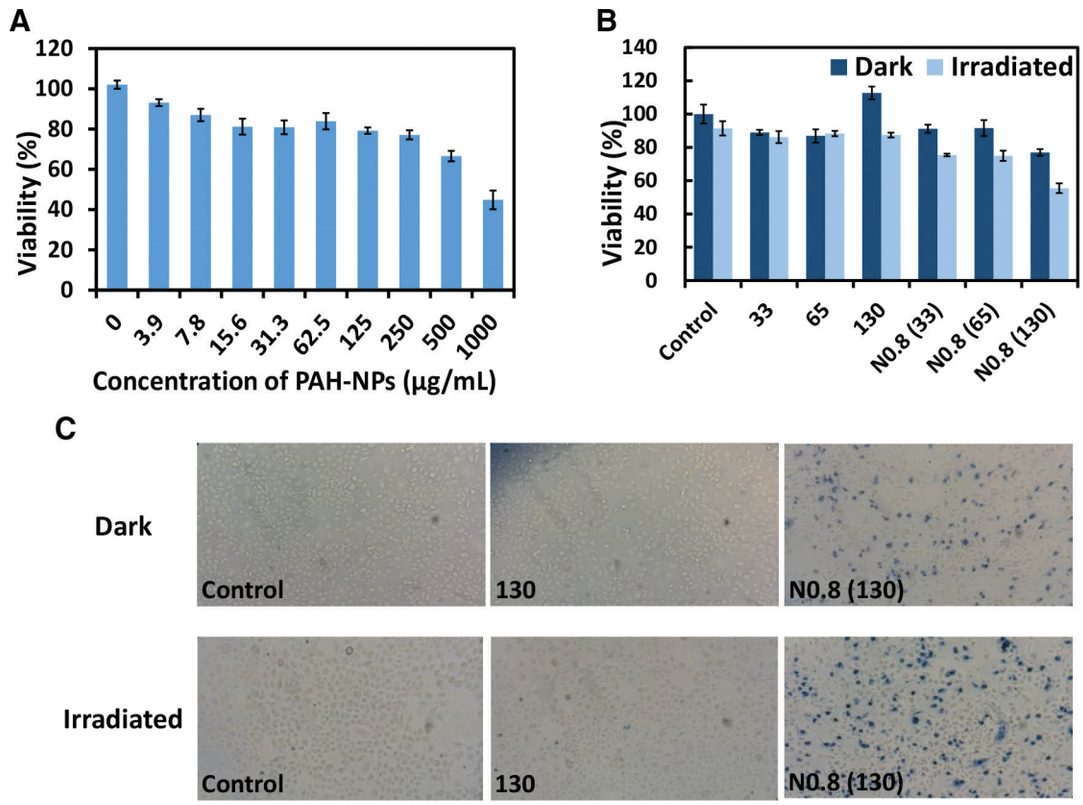

Fig. 7 In vitro tests of NPs. A, MTT assay was conducted using A549 cells. Cytotoxicity of PAH-coated NPs was calculated as the percentage decrease in the absorbance of formazan crystals compared with that of the unt-reated cells (n = 6). B, Photocytotoxicity of the RB-NPs was tested using A549 cells treated with either RB or RB-saturated RB-NPs (N0.8) for 4 h. After washing, the cells were exposed to ambient light for 30 min. CCK-8 was used to determine the cell viability. Data are mean ± SD (n = 4). The concentrations of RB-NPs used were 125, 250, and 500 μg/mL, which are similar to those of free RB solutions having concentrations of 33, 65, and 130 μM, respectively. Values in parentheses are the concentration of NP-bound RB (μM). C, Trypan blue was used to distinguish live and dead cells at 100-times of magnification. A549 cells were treated with either RB (130 μM) or 0.5 mg/mL of RB-NPs (N0.8). Before exposure to ambient light for 30 min, the cells were washed with PBS. Parentheses indicate the concentration of NP-bound RB (μM). CCK-8 = Cell Counting Kit-8; NP = nanoparticle; PAH = polyallylamine; PBS = phosphate-buffered saline; RB = rose bengal.

photocytotoxic effects of the RB-NPs also show their potential in PDT, although more efforts should be placed on how to modify the coat materials and lessen the bioactivities of the PAH coat.

REFERENCES

1. Brown SB, Brown EA, Walker I. The present and future role of photodynamic therapy in cancer treatment. *Lancet Oncol* 2004;**5**:497–508.
2. Wang B, Wang JH, Liu Q, Huang H, Chen M, Li K, et al. Rose-bengal-conjugated gold nanorods for in vivo photodynamic and photothermal oral cancer therapies. *Biomaterials* 2014;**35**:1954–66.
3. Croce AC, Wyroba E, Bottiroli G. Distribution and retention of rose bengal and disulphonated aluminium phthalocyanine: a comparative study in unicellular eukaryote. *J Photochem Photobiol B* 1992;**16**:318–30.
4. Estevão BM, Cucinotta F, Hioka N, Cossi M, Argeri M, Paul G, et al. Rose Bengal incorporated in mesostructured silica nanoparticles: structural characterization, theoretical modeling and singlet oxygen delivery. *Phys Chem Chem Phys* 2015;**17**:26804–12.
5. Dabrzalska M, Janaszewska A, Zablocka M, Mignani S, Majoral JP, Klajnert-Maculewicz B. Cationic phosphorus dendrimer enhances photodynamic activity of rose bengal against basal cell carcinoma cell lines. *Mol Pharm* 2017;**14**:1821–30.
6. Reineck P, Gómez D, Ng SH, Karg M, Bell T, Mulvaney P, et al. Distance and wavelength dependent quenching of molecular fluorescence by Au@SiO_2 core-shell nanoparticles. *ACS Nano* 2013;**7**:6636–48.
7. Zhang D, Nettles CB. A generalized model on the effects of nanoparticles on fluorophore fluorescence in solution. *J Phys Chem C* 2015;**119**:7941–8.
8. Shen J, Sun C, Wu X. Silver nanoprisms-based Tb(III) fluorescence sensor for highly selective detection of dopamine. *Talanta* 2017;**165**:369–76.
9. Aime S, Botta M, Terreno E. Gd (III)-based contrast agents for MRI. *Adv Inorg Chem* 2005;**57**:173–237.
10. Dong H, Du SR, Zheng XY, Lyu GM, Sun LD, Li LD, et al. Lanthanide nanoparticles: from design toward bioimaging and therapy. *Chem Rev* 2015;**115**:10725–815.
11. Janeesh P, Sami H, Dhanya C, Sivakumar S, Abraham A. Biocompatibility and genotoxicity studies of polyallylamine hydrochloride nanocapsules in rats. *RSC Adv* 2014;**4**:24484–97.
12. Li X, Wang R, Zhang F, Zhou L, Shen D, Yao C, et al. Nd3+ sensitized up/down converting dual-mode nanomaterials for efficient in-vitro and in-vivo bioimaging excited at 800 nm. *Sci Rep* 2013;**3**:3536–42.
13. Pan Y, Zhang L, Zeng L, Ren W, Xiao X, Zhang J, et al. Gd-based upconversion nanocarriers with yolk-shell structure for dual-modal imaging and enhanced chemotherapy to overcome multidrug resistance in breast cancer. *Nanoscale* 2016;**8**:878–88.
14. Wang JH, Wang B, Liu Q, Li Q, Huang H, Li S, et al. Bimodal optical diagnostics of oral cancer based on Rose Bengal conjugated gold nanorod platform. *Biomaterials* 2013;**34**:4274–83.
15. Nsubuga A, Mandl GA, Capobianco JA. Investigating the reactive oxygen species production of rose bengal and merocyanine 540-loaded radioluminescent nanoparticles. *Nanoscale Adv* 2021;**3**:1375–81.
16. Chen G, Ohulchanskyy TY, Liu S, Law WC, Wu F, Swihart MT, et al. Core/shell $NaGdF_4$:Nd3+/$NaGdF_4$ nanocrystals with efficient near-infrared to near-infrared downconversion photoluminescence for bioimaging applications. *ACS Nano* 2012;**6**:2969–77.
17. Baek NS, Kim YH, Kim HK. Rational design, exploratory synthesis and lanthanide emission efficiency comparison of lanthanide (III)-cored

complexes based on naphthalene acid ligands for efficient energy transfer pathways. *Bull Korean Chem Soc* 2006;**27**:1729–30.
18. Lucky SS, Soo KC, Zhang Y. Nanoparticles in photodynamic therapy. *Chem Rev* 2015;**115**:1990–2042.
19. Xu D, Neckers D. Aggregation of rose bengal molecules in solution. *J Photochem Photobiol A: Chem* 1987;**40**:361–70.
20. Doktorovova S, Shegokar R, Martins-Lopes P, Silva AM, Lopes CM, Müller RH, et al. Modified Rose Bengal assay for surface hydrophobicity evaluation of cationic solid lipid nanoparticles (cSLN). *Eur J Pharm Sci* 2012;**45**:606–12.
21. Mielke M, Zimehl R. Measures to determine the hydrophobicity of colloidal polymers. *Prog Colloid Polym Sci* 2001;**117**:56–62.
22. Sun X, Ji Z, He S. SHG-enhanced NIR-excited in vitro photodynamic therapy using composite nanoparticles of barium titanate and rose Bengal. *RSC Adv* 2019;**9**:8056–64.
23. Stallivieri A, Baros F, Arnoux P, Vanderesse R, Barberi-Heyob M, Frochot C. Production of singlet oxygen by nanoparticle-bound photosensitizers. In: Nonell S, Flors C, editors. *Comprehensive series in photochemical & photobiological sciences*. 1st ed. London, United Kingdom: Royal Society of Chemistry; 2016, p. 209–23.
24. Serrano MP, Rafti M, Thomas AH, Borsarelli CD. Photosensitizing properties of hollow microcapsules built by multilayer self-assembly of poly(allylamine hydrochloride) modified with rose Bengal. *RSC Adv* 2019;**9**:19226–35.
25. Kuznetsova NA, Gretsova NS, Derkacheva VM, Kaliya OL, Lukyanets EA. Sulfonated phthalocyanines: aggregation and singlet oxygen quantum yield in aqueous solutions. *J Porphyr Phthalocyanines* 2003;**7**:147–54.
26. Alekseenko L, Shilina M, Kozhukharova I, Lyublinskaya O, Fridlyanskaya I, Nikolsky N, et al. Impact of polyallylamine hydrochloride on gene expression and karyotypic stability of multidrug resistant transformed cells. *Cells* 2020;**9**:2332–49.
27. Rudt A, Sun J, Qin M, Liu L, Syldatk C, Barbeck M, et al. Controlled adhesion of HUVEC on polyelectrolyte multilayers by regulation of coating conditions. *ACS Appl Bio Mater* 2021;**4**:1441–9.
28. Jin J, Gu YJ, Man CW, Cheng J, Xu Z, Zhang Y, et al. Polymer-coated $NaYF_4$:Yb^{3+}, Er^{3+} upconversion nanoparticles for charge-dependent cellular imaging. *ACS Nano* 2011;**5**:7838–47.
29. Xu J, Kuang Y, Lv R, Yang P, Li C, Bi H, et al. Charge convertibility and near infrared photon co-enhanced cisplatin chemotherapy based on upconversion nanoplatform. *Biomaterials* 2017;**130**:42–55.
30. Liang L. *Biofunctional Upconversion Nanoparticles for Cancer Theranostics*. *PhD Thesis*, Macquarie University, Sydney, 2016.
31. Mi P. Stimuli-responsive nanocarriers for drug delivery, tumor imaging, therapy and theranostics. *Theranostics* 2020;**10**:4557–88.
32. Chung YC, Wei MF, Chang FH, Young TH. PEGylated guanidinylated polyallylamine as gene-delivery carrier. *J Biomater Sci Polym Ed* 2011;**22**:1829–43.
33. Kamkaew A, Chen F, Zhan Y, Majewski RL, Cai W. Scintillating nanoparticles as energy mediators for enhanced photodynamic therapy. *ACS Nano* 2016;**10**:3918–35.